Nanoscale

Accepted Manuscript

This article can be cited before page numbers have been issued, to do this please use: N. N. Jason, S. J. Wang and W. Cheng, *Nanoscale*, 2016, DOI: 10.1039/C6NR04056J.

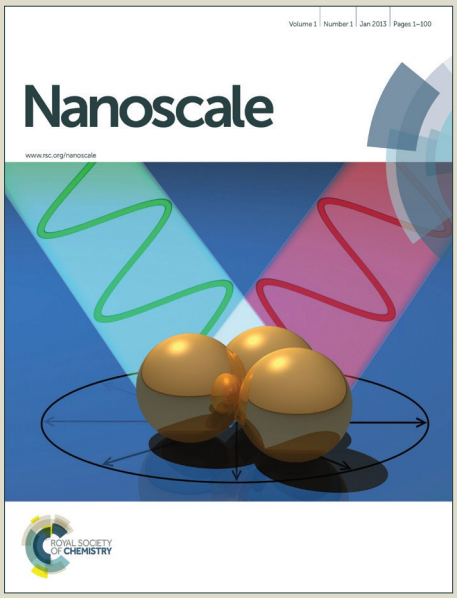

View Article Online
DOI: 10.1039/C6NR04056J

Nanoscale

ARTICLE

Skin Inspired Fractal Strain Sensors Using a Copper Nanowires and Graphite Microflakes Hybrid Conductive Network

N. N. Jason,[a] S. J. Wang,[bc] and W. Cheng[d]

Received 00th January 20xx,
Accepted 00th January 20xx

DOI: 10.1039/x0xx00000x

www.rsc.org/

This work demonstrates a facile "Paint-On" approach to fabricate highly stretchable and highly sensitive strain sensors by combining one-dimensional copper nanowires networks with two-dimensional graphite microflakes. This paint-on approach allows for fabrication of electronic skin (e-skin) patches which can directly replicate with high fidelity the human skin surface they are on, regardless of topological complexity. This leads to high accuracy for detecting biometric signals for applications in personalised wearable sensors. The copper nanowires contribute to high stretchability and the graphite flakes offer high sensitivity, and their hybrid coating offers the advantages of both. To understand topological effects on sensing performance, we utilizes fractal shaped elastomeric substrates and systematically compared their stretchability and sensitivity. We could achieve a high stretchability of up to 600% and a maximum guage factor of 3000. Our simple yet efficient paint-on approach enabled facile fine-tuning of sensitivity/stretchability simply by adjusting ratios of 1D vs. 2D materials in the hybrid coating, and the topological structural designs. This capabilty leads to a wide range of biomedical sensors demonstrated here, including pulse sensor, prosthetic hand, and a wireless ankle motion sensor.

Introduction

We can think of the human skin as a pre-strained and therefore wrinkled elastic sheet. This facilitates biaxial strain by deforming in such a way that majority of the strain is converted to compressional stress and thereby avoiding tears from forming on the skin due to excess longitudinal strain concentration in isolated areas. In elastic sheets, on increasing the aspect ratio (α = L/W), where L = length and W = width of the sheet before strain, there is a transition where majority of the forces experienced by the sheet turn to more of compressional stresses perpendicular to the width and less of longitudinal strains along the length, and vice versa.[1] This allows a high α sheet to endure extremely large strains without tearing. It must be noted that the sheet is clamped at the two ends of the length of the sheet, with the clamp being at least as wide as the sheet itself. In essence, human skin has a typical stretchability of less than 30%, but it is still able to protect the body from injury by continuous monitoring of strain, pressure and temperature over the entire skin surface, especially the injury prone areas such as the joints.[2]

Much of the research work in this field was primarily based on simple patch based architectures with various nanomaterial based inks as the sensing element for strain detection.[3-12] Examples include interlocking fibres, lateral un-entangling of carbon nanotubes for strain sensing or gold nanowires soaked tissue paper peizoresistive pressure sensors, etc.[13-18] It has been demonstrated that multi-functionality in a single setup was possible by using rigid silicon in the form of thin serpentine shavings and connected them to microelectronic components to fabricate a tattoo-like, skin attachable, plethora of integrated devices including self-similar or fractal interconnects, strain, temperature, and electrostatic potential (EP) sensors.[18-22] Complex functions such as cardio therapy have also been achieved using the same strategy.[23] Building on this concept, there has also recently been a "cut-and-paste" e-skin which actually doesn't utilize any nanomaterials at all, and instead uses commercially available metallic thin films.[9, 24] There have also been some novel 3-D printed architectures to fabricate E-Skins.[25]

Despite the significant progress in e-skin sensors, majority of them are made by fabrication of sensors first and attachment to skin later. This strategy couldn't replicate human skin surface textures with high fidelity, limiting their applications in personalised wearable electronics. Here, we describe a simple yet efficient 'paint-on' strategy which can circumvent this limitation, by using graphite microflakes (GrMFs) and copper nanowires (CuNWs) as the conducting/sensing elements. Although CuNWs do tend to oxidise rapidly when exposed to air, this problem can be easily solved by using nickel based protective alloy shells on the NWs.[12, 26, 27] The combination of GrMFs and CuNWs enables facile tuning of desired sensitivity and stretchability. We could paint sensors directly on human skin, fabric and other complex surfaces as required by the

[a] Department of Chemical Engineering, Faculty of Engineering, Monash University, Clayton 3800, Victoria, Australia.
[b] International Tangible Interaction Design Lab (ITIDLab), Monash University, Clayton, Victoria 3800, Australia
[c] Interaction Design, Department of Design, Faculty of Art Design and Architecture, 900 Dandenong Road, Caulfield East 3145, Victoria, Australia.
[d] Department of Chemical Engineering, Faculty of Engineering, Monash University, Clayton 3800, Victoria, Australia.
Electronic Supplementary Information (ESI) available: Supporting information images S1-S8 and videos S1-S3. See DOI: 10.1039/x0xx00000x

View Article Online
DOI: 10.1039/C6NR04056J

end user. As a result of being free from complex fabrication methods, the user has the freedom to manufacture a wide range of sensors with varying sensitivities and stretchabilities on virtually any substrate; regardless of topological complexity. In addition to materials-based tuning, we could extend the stretchability by combining fractal design.[21, 22, 28, 29] With optimum design, we could achieve a high stretchability of up to 600% and a maximum guage factor of 3000. The wearable sensors on skin can be easily washed away by water after use, and the smart sock can simply be removed like a normal sock and discarded as well. The total cost including the conductive paint, elastomeric substrates and sealants and the conductive thread per sensor is estimated to be less than AUD $2. Moreover, the paintable sensors can be seamlessly integrated with wireless networks for continuous, real time biometric data collection, transmission and sharing.

To demonstrate the biomonitoring capabilities of the sensors the GrMFs ink was directly painted onto the human skin and the resulting sensor was used to measure the ankle brachial pulse from the Posterior Tibial Artery. A single sensor was also painted on the wrist and it could distinctly detect individual finger motions, palm flexion and extension. Finally, a group of three sensors using the GrMFs/CuNWs/GrMFs ink was painted around the ankle; front and on both sides to monitor the Calcaneo-Fibular, Medial, and the Anterior-Tibiofibular ligaments. The sensors were painted on a sock and coupled with a wireless platform to demonstrate a truly wearable and wire-free, untethered sensor package for sporting applications. This was used to collect real time ankle motion data simultaneously from all three sensors on a smart phone.

Results and Discussion

The fabrication process for the sensors begins first with the synthesis of the CuNWs and GrMFs inks. The aqueous CuNWs ink was made using the methodology specified in our previous work,[9] and the GrMFs ink was made by dissolving shavings of a commercial 9B water soluble graphite crayon in water. Both types of inks could be painted on elastomers. We thoroughly investigated their ink-on-elastomer behaviours with respect to applied strain. Three types of percolation networks formed here, namely, a CuNWs based network made of one dimensional nanowire building blocks, a GrMFs network made of two dimensional flakes arranged onto each other like scales on reptilian skin, and finally a hybrid network comprising the GrMFs/CuNWs/GrMFs sandwich structure.

The NWs based network has been thoroughly researched in previous reports. The deformation ability of the NWs dictate whether the change in resistance in a NWs network comes from contact resistance, breaking of contact entirely between nanowires due to out of plane buckling and overstretching of the NWs film. Moreover, if the NWs are bound to each other and the elastomer substrate quite rigidly then the resistance changes are due to formation of cracks in the percolation network during strain. Figure 1(a) shows the uniform network of CuNWs formed before the application of strain, but under application of 50% strain we can see cracks in the NWs film perpendicular to the direction of strain, as shown in Figure 1(b) outlined in the red dashed box and also seen in Figure S1. The formation of compressional wrinkles parallel to the direction of strain are also clearly visible, Figure S1(a, b, c). This is a very clear example of the Poisson effect in play. Upon relaxation of the strain the cracks close up, but a seamless smooth film is not formed, Figure 1(c). This illustrates that NWs films are inherently prone to degrading due to their inability to return to their original positions post deformation, which is consistent with previous NW-based systems.[8, 30, 31]

The GrMFs form a percolation network in a different fashion. The conductive film is constructed of the flakes overlapping each other. Figure 1(d) shows that the surface is relatively smooth without observing the overlapping layers of graphite flakes. Under 50% strain, the graphite flakes separate from the layers below partly to accommodate the deformation Figure 1(e), and after removal of strain fall back into their original positions similar to the previous reports.[32] The new surface shows ridges where the flakes separated out, Figure 1(f). The loosely stacked GrMFs slided over each other when under strain, and returned to their initial positions upon stress relaxation. This is analogous to the naturally existing biological scales of animals (e.g. reptiles or fish) which slide over each other when the animal is navigating complex turns and motions. This is why GrMFs are ideal for maintaining electrical contact while undergoing any kind of deformation.

The GrMFs/CuNWs/GrMFs percolation network was prepared by layer-by-layer coating, which is in essence the two aforementioned networks in a sandwich form. The hybrid coating, Figure 1(g) has a topology similar to Figure 1(d) due to the GrMFs coating being the final layer in both cases. The cracking behaviour after the application of 50% strain is similar to GrMFs film as well, but in the crevices formed by the sliding graphite layers we can see the CuNWs layer acting as a percolation network bridge, Figure 1(h). Upon relaxation of the strain the cracks close up, much like the earlier observed coatings. So when the GrMFs slide over each other like the scales on reptilian skin and expose a gap, the CuNWs bridge the gap taking advantage of their long length.

The unsealed samples in Figure 1 exhibit cracking and tearing but this behaviour is diminished to a very large extent when the samples are sealed with a commercial transparent adhesive rubber strip. For instance, the stretchability range of the linear CuNWs sensor could be extended from ~50% to ~280% after rubber sealing. However, the electrical signals still degraded during the 10,100 cycles durability test at 10% strain as shown in Figure 2(a). As for GrMFs, Figure 2(b), sudden spikes and irregular peaks were observed now and then, although generally remaining more stable than the CuNWs coating. In contrast, the hybrid film with sealing, Figure 2(c) clearly shows the clean signal from the CuNWs combined with the stability of the GrMFs network. The signal deterioration observed for the CuNWs was also greatly diminished with the hybrid coating. This demonstrated that sealing greatly enhances strain range, whereas a hybrid conductive coating

View Article Online
DOI: 10.1039/C6NR04056J

improves signal quality by taking advantage of the properties of the individual coatings.

To determine the best material or materials combination to detect accurately quick, sharp or minute movements, the sensors with five different conductive coatings; CuNWs, GrMFs, GrMFs/CuNWs/GrMFs, Gr2MFs/CuNWs/GrMFs, GrMFs/Cu2NWs/GrMFs, were stretched at varying frequencies and the average current changes for each coating was plotted. The number "2" after GrMFs and CuNWs signify two coatings. The sensors were stretched at 1.5, 2.5 and 3 Hz at 1% strain for 100 cycles. It is obvious from Figure 3(a, b, c) that irrespective of frequency the GrMFs coating has the highest sensitivity, whereas the CuNWs the lowest. The GrMFs/CuNWs/GrMFs coatings perform only marginally better than the CuNWs coating, while the rest of the coatings perform slightly better than the previous hybrid coating owing to the increased GrMFs and CuNWs coatings.

As the CuNWs coating and the GrMFs coating have distinct curve shapes during the cyclic tests, so it is possible to determine the material playing the dominant role in sensing strain. The visual representation of the dominant materials in a hybrid coating is shown in Figure S2. In Figure S2(a) the CuNWs coating we can see two broad peaks with two small peaks together in the valley region at the beginning and the middle of the curve at 1.5 Hz. At 2.5 Hz one of the valley peaks has vanished, and at 3 Hz all the peaks become defined and regular. The valley peaks may be attributed to the sharp movements that the linear translation stage motor generates when changing direction for to and fro motion, and the tall peaks are the changes reflected for the strain. For the GrMFs coating, we see pointier peaks reflecting the higher sensitivity of the coating as shown in Figure S2(b). The twin valley peaks in this case survive the 2.5 Hz frequency but one of them is lost at 3 Hz. The curve at Figure S2(c) for the GrMFs/CuNWs/GrMFs coating looks like the averaged out value embodying characteristics of both CuNWs and GrMFs coatings. The hybrid curve contains all the peaks that exist at the particular frequency for both the individual component coatings. With an extra coat of GrMFs the hybrid curve in Figure S2(d) has more in similar with Figure S2(b), whereas with an extra CuNWs coat the Figure S2(e) looks no different from Figure S2(c). With the increase in frequency the jerks are much less pronounced, therefore the loss of peaks may not necessarily reflect loss of sensitivity.

To reveal how the conductive coating influences the strain range of a sensor it is necessary to find the failure strain limit of the particular coating. The three conductive inks were painted on a linear sensor and stretched to failure i.e. infinite resistance reading. The GrMFs had a limit of 30%, the hybrid coating 70% and the CuNWs at 280%, Figure 3(d). It is obvious that the extraordinary strain range is the strength of the CuNWs coating and as proven in Figure 3(a, b, c), while the extremely high sensitivity is the strength of the GrMFs, as also seen in Figure S3. The strain range of the hybrid coatings are found to be a compromise between the former individual coatings.

It is expected that wrinkles on skin will influence its sensitivity and stretchability to external strains. To understand this, we fabricated sensors with a few basic first order fractal shapes, namely linear, zigzag, serpentine, and square shape. These shaped sensors were supported on latex substrates as shown in Figure 4(a, b, c). Then CuNWs ink was painted and dried on the substrates at room temperature, and finally sealed with a commercial transparent adhesive rubber tape. The α(s) of the shapes were measured to be linear-6.6, zigzag-8.3, serpentine-10.6, square-14.3. The various shapes have different α(s), and therefore the Poisson effect affects them differently as well. The shrinkage in width of the latex substrate due to transversal compression during strain occurs in the following order, linear>zigzag>serpentine>square. As is evident from the images the linear shape is affected the most, followed by the zigzag shape, and as the square shape is stiffer than the serpentine shape because of its angularity so it is more susceptible than the serpentine shape. It should also be noted that the shapes that undergo out-of-axis displacement; square and serpentine, are more compliant to strain than the other shapes. Theoretically, the more angles a shape has the more tensile stiffness it will have. Hence, the descending order of tensile stiffness for the fractal shapes are, square > zigzag > serpentine, with the linear shape being most stiff due to its non-fractalness.

Another aspect to be noted here is that the tensile stiffness maybe reduced by increasing the number of bends in the fractal i.e. using a higher order fractal.[21, 22, 33] In relation to the conductive coatings, a high tensile stiff shape will result in a higher sensitivity but a lower strain range and vice versa. This is due to lesser tolerance for strain by the shape and early failure of the conductive coating. The linear sensor with the smallest α endures the maximum effect of the Poisson effect which renders the conductive coating to be greatly affected. This causes the sensitivity to be the highest in the below 10% strain ranges, and the ultimate strain to be the least of all shapes. On the contrary, the square shaped sensor which has the largest α absorbs much of the strain through out of plane twisting. But owing to its angularity is rendered stiffer, hence it shows the second largest strain range at almost 450% instead of the serpentine shape which despite having a lower α = 10.6 has a higher strain range at 600%. The zigzag shape has a low α = 8.3 and is also angular, hence it is ranked after the linear shape in terms of stretchability.

Apart from shape, the conductive coating used also decides the strain range and the sensitivity for a strain sensor. Therefore the sensors' sensitivities within a strain range with respect to the shapes and coatings have been thoroughly investigated. As is evident in the strain range comparison histograms between different fractal shapes for the three coatings Figure 4(d,e,f) CuNWs coatings while displaying the highest strain ranges; 600% for the serpentine shape have the lowest sensitivities among the shapes. Whereas, the GrMFs coatings have the lowest strain ranges; only 30% for the linear shape, but the highest sensitivities. The sandwich percolation networks of the GrMFs/CuNWs/GrMFs coatings show averaged out characteristics between CuNWs and GrMFs. The corresponding curves showing the ultimate strains at which

View Article Online
DOI: 10.1039/C6NR04056J

the sensors fail are depicted in Figure S3. The hybrid coatings' strain limit always lies within the limits of the other two coatings. Figure S4 also displays this trend of increasing strain range in terms of shapes and conductive coatings.

The effect of tensile stiffness of the wave shapes used was confirmed for two dimensional patterns as well. Rows of the zigzag, square and the serpentine wave shapes were laid orthogonally to each other to construct second order fractal patterns, shown in Figure 5(a, b, c). The insets show the respective first and second order patterns. These patterns allow for biaxial stretching and torsion. Figure 5(d) shows that there is a large difference between the resistance changes for strain along the "X"- ε(11) and "Y"- ε(22) axes for the zigzag shape. The difference is much lesser in comparison to the square shape, and the least, almost overlapping for the serpentine shape. It is also observed in the torsion - ε(12) test, Figure 5(e) that the peak value for resistance changes is the highest for the zigzag shape, followed by square, and serpentine. This shows that according to the trend of the Poisson effect influenced by fractalness of the shapes; zigzag>square>serpentine, the more fractal a shape is, the lesser it will be directly affected by biaxial strain and torsion. The majority of the applied strain will be spent in uncoiling the fractal, like a spring.

For biomedical monitoring, strain based plethysmographic changes in the human skin over areas of interest in the human body are measured, such as the skin over arteries, muscles, joints and so on. These kinds of measurements require that the sensitivity be high in the respective strain ranges. For instance, a blood pulse will typically generate an under 1% strain change, therefore either the GrMFs or the GrMFs/CuNWs/GrMFs linear sensors with a GF ~36. Similarly, for measuring proprioceptive musculoskeletal movements the zigzag wave shape sensor having a GF ~ 6 for the GrMFs coating or GF ~ 11 for Gr MWs/CuNWs/GrMFs within the 20-60% strain range would be suitable. For strains in the vicinity of 100% both coatings except the CuNWs coating show a GF ~100 regardless of shape of the sensors. Beyond 100% strain the sensors reach a sensitivity upwards of GF ~1000. The amount of detailed minute movements that can be detected by a particular combination of a fractal shape and conductive coating i.e. demonstrated in Figure S5. In general the zigzag, serpentine and square are the most sensitive in picking up movements. But when they are coated with CuNWs, all of them show low sensitivity, and look more or less the same. When the shapes are coated with the hybrid coating it was observed that the signal becomes cleaner and more regular. This was especially evident in the linear shape. This demonstrates that it is possible to tailor the sensor to have its highest sensible region in the strain range we desire by using a suitable fractal shape and conductive coating.

We further demonstrate that a coating of CuNWs, GrMFs and a combination thereof could adhere on an ecoflex replica of the human skin with high fidelity. Figure 6(a) shows the ecoflex skin coated with CuNWs, Figure 6(c) with GrMFs and Figure 6(e) GrMFs with a coating of CuNWs over it, and Figure 4(b, d, f) depict the respective magnifications. It should be noted that for the experiments and measurements a sandwich of GrMFs/CuNWs/GrMFs was used. Figure 6(e) doesn't include the third layer of GrMFs to enunciate visually the placement of the CuNWs on the GrMFs layer underneath, and during experiments between the layers of GrMFs. It can be observed that the nanomaterials drape over the many wrinkles and crevices on ecoflex skin. This shows how the conductive paint is able to accurately replicate the contours of the skin. Figure 6(d) shows how the GrMFs bind tightly to each, almost merging into each other. It is also interesting to note that when the graphite is made into an aqueous paint, it is only then that the microflakes settle into a tightly bound snake-skin scale like arrangement. The water seems to have an intercalating effect at the micron level if not at the nano level and separate out multilayered graphene flakes. The same intercalating effect doesn't happen with rubbing the graphite on a surface as done with a pencil, as shown in Figure S6.

As demonstrated above, our 'paint-on' approach could potentially lead to personalised wearable sensors conformal to local skin textures with adjustable sensitivities and stretchabilities. This displays the potential in monitoring a wide range of biometric signals. The GrMFs was painted as a single patch directly on the inner wrist and then sealed with a transparent adhesive rubber strip, Figure S7(a), and this sensor was used to detect skin strains caused by the movement of the tendons underneath. The sensor is able to detect each finger movement distinctly, followed by palm flexion and extension, Figure 7(a). Each movement was made twice to show reproducibility. This could be potentially used as a prosthetic interface for hand amputees. The GrMFs was also painted onto the posterior tibial artery site to detect the ankle brachial pulse, Figure 7(b) like a tattoo in the shape of a bat, Figure S7(b). The sensor could very easily pick up the early systolic (p1), late systolic (p2) pressure peaks, and even the dicrotic notch (p3) in the pulse wave, shown in the inset. The demonstration can be viewed in supporting information video S1. The ability to avoid intrusive catheter based methods or uncomfortable pressure cuff based methods in favour of a facile paintable pulse sensor has huge implications in the medical field. Ideally, for measuring pulse wave velocity the carotid artery on the neck and any other artery site on the body's extremities would give a very accurate read out. But due to the discomfort of having a pressure cuff on the neck, the arms and the legs are chosen as the measurement sites. Now, the availability of a non-intrusive, imperceptible paintable strain sensor allows for applying sensors on any artery site on the body with no discomfort.

The GrMFs/CuNWs/GrMFs paint were painted on a sock and positioned such that the skin strains caused by the Calcaneo-fibular, Medial, and the Anterior-tibiofibular ligaments respectively could be measured. The schematic, Figure 8(a) shows how the three sensors are connected to a wireless platform which can communicate with a mobile device and show real time data while the ankle is in motion. This sock is an ideal wearable sensor platform designed to monitor ankle movement during sporting actions in real time. The inset images illustrate what kind of positions of the ankle would risk causing a torn ligament. Figure 8(b,c,d,e) depict the raw data collected from the ankle for the respective foot motions. Each movement was made three times to

View Article Online
DOI: 10.1039/C6NR04056J

demonstrate consistency of the measurements. Each set of waveforms is distinct for each movement. This setup is ideal for sporting, physiotherapy and rehabilitation based applications.[34] This is aimed at injury prevention by accurate proprioceptive knowledge of the ankle during motion. The demonstration of this sensor can be viewed in supporting information videos S2 and S3.

Conclusions

In conclusion, this work represents a thorough study of various conductive coatings; CuNWs, GrMFs and the combinations there of, on the latex substrates and their behaviour under strain. The different shaped latex substrates; linear, zigzag, serpentine, and square, add another layer of tunability by introducing aspect ratio and Poisson effect based deformations and their effect on the conductive coatings. Using the facile "paint-on" approach it is possible to develop e-skin sensors which can directly be fabricated on the human skin hence giving us a high fidelity, and user specific skin replica of the surface topology. This enables us to have high accuracy for biometric data collection. Within the 10% range a very high GF~36 and a maximum GF~3000 overall was displayed by the sensors, which is well suited for a plethora of applications including biomonitoring, prosthetic and sporting applications. The extremely high stretchability of 600% again offers applications in the robotics area. All the sensors have displayed a durability of 10,000 cycles at 10% strain, Figure S8. The facile fabrication route, robustness, and the economically viable nature of the "paintable" sensors makes it ideal for healthcare needs in developing nations. The "paintable" and "wireless" nature of the sensors allows for a cuff free measurement and collection of blood pulse and plethysmography data. This is especially advantageous for infants and geriatric patients. The GrMFs based sensors may be immediately deployed for this cause.

Experimental section

Materials. Hydroxypropyl cellulose (HPC) Sigma-Aldrich, 20 mesh, Mw = 1 000 000, Hexadecylamine (HDA) Sigma-Aldrich, D-glucose (α or β) Merck, Copper chloride ($CuCl_2 \cdot 2H_2O$) Sigma-Aldrich, LYRA water soluble graphite crayons 9B.

CuNWs Synthesis. The CuNWs were synthesized using a modified earlier published method.[35] 50 mL of water was heated to 100 °C. Then 900 mg of hexadecylamine (HDA) and 100 mg of copper chloride ($CuCl_2 \cdot 2H_2O$) were added and stirred for 20 min at 1000 rpm. When solution turns into homogeneous sky blue color, then add 500 mg of D-glucose (α or β) (Merck) and the stirring speed was reduced to 400 rpm. The solution gradually changed colour from pale brown to dark brown. The reaction was stopped after 6 hours. The solution was removed from the oil bath and was cooled at room temperature for 10 min after which it was centrifuged at 6500 rpm for 5 min. The CuNWs collect at the bottom of the tubes as a pellet, which was recovered by carefully decanting the supernatant and gently rinsing with Mili-Q water a few times. The CuNWs formed are 25-35 nm in diameter and 50-60 µm long.

CuNWs Ink Formulation. 1 gm (wet pellet weight) of CuNWs, 9.468 mg of HPC, and 2.2 ml of Mili-Q water were blended well to make the ink.

GrMFs Ink Formulation. 300 mg of shavings from a water soluble graphite crayon were dissolved in 20 µL of Mili-Q water to make the ink. The GrMFs are < 10 µm in diameter and the thickness can be anywhere between few 100 nm to 1 µm depending on the number of layers.

Characterization. High-resolution images of the CuNWs were captured using the FEI Nova NanoSEM 450 FESEM.

Sensor Fabrication. The elastomer substrates are prepared by pouring liquid latex into 3D printed moulds and then curing at 70°C for 30 minutes. The conductive threads were stuck on the ends of the sensors as electrodes using liquid latex. The required conductive paint was painted on the top surface of the sensor using a paintbrush. After drying of the assembly, the dried paint was sealed on the sensor using commercial transparent stretchable medical rubber tape, OPSITE FLEXIFIX.

Acknowledgements

The research has been funded by the Australian Research Council DP15013750. This work was performed in part at the Melbourne Centre for Nanofabrication (MCN) in the Victorian Node of the Australian National Fabrication Facility (ANFF). The authors acknowledge use of the microscopy facilities within the Monash Centre for Electron Microscopy (MCEM). The author NNJ also wish to acknowledge the Victorian International Research Scholarship (VIRS) for their support.

References

[1] V. Nayyar, K. Ravi-Chandar, R. Huang, International Journal of Solids and Structures 2011, 48, 3471.
[2] V. Arumugam, M. D. Naresh, R. Sanjeevi, Journal of Biosciences 1994, 19, 307.
[3] S. Gong, D. T. H. Lai, B. Su, K. J. Si, Z. Ma, L. W. Yap, P. Guo, W. Cheng, Advanced Electronic Materials 2015, 1, n/a.
[4] S. Gong, D. T. Lai, Y. Wang, L. W. Yap, K. J. Si, Q. Shi, N. N. Jason, T. Sridhar, H. Uddin, W. Cheng, ACS Appl Mater Interfaces 2015, 7, 19700.
[5] L. Cai, L. Song, P. Luan, Q. Zhang, N. Zhang, Q. Gao, D. Zhao, X. Zhang, M. Tu, F. Yang, W. Zhou, Q. Fan, J. Luo, W. Zhou, P. M. Ajayan, S. Xie, Sci Rep 2013, 3, 3048.
[6] S.-H. Bae, Y. Lee, B. K. Sharma, H.-J. Lee, J.-H. Kim, J.-H. Ahn, Carbon 2013, 51, 236.
[7] Y. Wang, T. Yang, J. Lao, R. Zhang, Y. Zhang, M. Zhu, X. Li, X. Zang, K. Wang, W. Yu, H. Jin, L. Wang, H. Zhu, Nano Research 2015, 8, 1627.
[8] M. Amjadi, A. Pichitpajongkit, S. Lee, S. Ryu, I. Park, ACS nano 2014, 8, 5154.

View Article Online
DOI: 10.1039/C6NR04056J

[9] N. N. Jason, W. Shen, W. Cheng, ACS Applied Materials & Interfaces 2015, 7, 16760.
[10] X. Li, R. Zhang, W. Yu, K. Wang, J. Wei, D. Wu, A. Cao, Z. Li, Y. Cheng, Q. Zheng, R. S. Ruoff, H. Zhu, Sci Rep 2012, 2, 870.
[11] J. Song, H. Zeng, Angew Chem Int Ed Engl 2015, 54, 9760.
[12] J. Song, J. Li, J. Xu, H. Zeng, Nano Lett 2014, 14, 6298.
[13] G. Schwartz, B. C. Tee, J. Mei, A. L. Appleton, H. Kim do, H. Wang, Z. Bao, Nat Commun 2013, 4, 1859.
[14] Y. Wang, L. Wang, T. Yang, X. Li, X. Zang, M. Zhu, K. Wang, D. Wu, H. Zhu, Advanced Functional Materials 2014, 24, 4666.
[15] T. Yamada, Y. Hayamizu, Y. Yamamoto, Y. Yomogida, A. Izadi-Najafabadi, D. N. Futaba, K. Hata, Nat Nanotechnol 2011, 6, 296.
[16] S. Gong, W. Schwalb, Y. Wang, Y. Chen, Y. Tang, J. Si, B. Shirinzadeh, W. Cheng, Nat Commun 2014, 5, 3132.
[17] C. Pang, G. Y. Lee, T. I. Kim, S. M. Kim, H. N. Kim, S. H. Ahn, K. Y. Suh, Nat Mater 2012, 11, 795.
[18] S. Lim, D. Son, J. Kim, Y. B. Lee, J.-K. Song, S. Choi, D. J. Lee, J. H. Kim, M. Lee, T. Hyeon, D.-H. Kim, Advanced Functional Materials 2015, 25, 375.
[19] W. H. Yeo, Y. S. Kim, J. Lee, A. Ameen, L. Shi, M. Li, S. Wang, R. Ma, S. H. Jin, Z. Kang, Y. Huang, J. A. Rogers, Adv Mater 2013, 25, 2773.
[20] R. C. Webb, A. P. Bonifas, A. Behnaz, Y. Zhang, K. J. Yu, H. Cheng, M. Shi, Z. Bian, Z. Liu, Y. S. Kim, W. H. Yeo, J. S. Park, J. Song, Y. Li, Y. Huang, A. M. Gorbach, J. A. Rogers, Nat Mater 2013, 12, 938.
[21] S. Xu, Y. Zhang, J. Cho, J. Lee, X. Huang, L. Jia, J. A. Fan, Y. Su, J. Su, H. Zhang, H. Cheng, B. Lu, C. Yu, C. Chuang, T. I. Kim, T. Song, K. Shigeta, S. Kang, C. Dagdeviren, I. Petrov, P. V. Braun, Y. Huang, U. Paik, J. A. Rogers, Nat Commun 2013, 4, 1543.
[22] J. A. Fan, W. H. Yeo, Y. Su, Y. Hattori, W. Lee, S. Y. Jung, Y. Zhang, Z. Liu, H. Cheng, L. Falgout, M. Bajema, T. Coleman, D. Gregoire, R. J. Larsen, Y. Huang, J. A. Rogers, Nat Commun 2014, 5, 3266.
[23] D.-H. Kim, R. Ghaffari, N. Lu, S. Wang, S. P. Lee, H. Keum, Proceedings of the National Academy of Sciences 2012, 109, 19910.
[24] S. Yang, Y. C. Chen, L. Nicolini, P. Pasupathy, J. Sacks, S. Becky, R. Yang, S. Daniel, Y. F. Chang, P. Wang, D. Schnyer, D. Neikirk, N. Lu, Adv Mater 2015.
[25] J. T. Muth, D. M. Vogt, R. L. Truby, Y. Menguc, D. B. Kolesky, R. J. Wood, J. A. Lewis, Adv Mater 2014, 26, 6307.
[26] A. R. Rathmell, M. Nguyen, M. Chi, B. J. Wiley, Nano Lett 2012, 12, 3193.
[27] I. E. Stewart, A. R. Rathmell, L. Yan, S. Ye, P. F. Flowers, W. You, B. J. Wiley, Nanoscale 2014, 6, 5980.
[28] A. Clausen, F. Wang, J. S. Jensen, O. Sigmund, J. A. Lewis, Advanced Materials 2015, 27, 5523.
[29] M. Park, J. Im, M. Shin, Y. Min, J. Park, H. Cho, S. Park, M. B. Shim, S. Jeon, D. Y. Chung, J. Bae, J. Park, U. Jeong, K. Kim, Nat Nanotechnol 2012, 7, 803.
[30] Y. Tang, S. Gong, Y. Chen, L. W. Yap, W. Cheng, ACS Nano 2014, 8, 5707.
[31] Y. Won, A. Kim, W. Yang, S. Jeong, J. Moon, NPG Asia Materials 2014, 6, e132.
[32] M. Hempel, D. Nezich, J. Kong, M. Hofmann, Nano Lett 2012, 12, 5714.
[33] Y. Su, S. Wang, Y. Huang, H. Luan, W. Dong, J. A. Fan, Q. Yang, J. A. Rogers, Y. Huang, Small 2015, 11, 367.
[34] S. J. Wang, Fields Interaction Design (FID): The answer to ubiquitous computing supported environments in the post-information age, Homa & Sekey Books, 2013.
[35] M. Jin, G. He, H. Zhang, J. Zeng, Z. Xie, Y. Xia, Angew Chem Int Ed Engl 2011, 50, 10560.

View Article Online
DOI: 10.1039/C6NR04056J

Figure 1. Optical images of (a) CuNWs, (d) GrMFs, (g) CuNWs/GrMFs, before strain. Images (b, e, h) are during 50% strain respectively, and (c, f, i) after strain respectively. The inset SEM images show the magnified view of the surface texture, and the material distribution visible through the cracks during strain and after removal of strain.

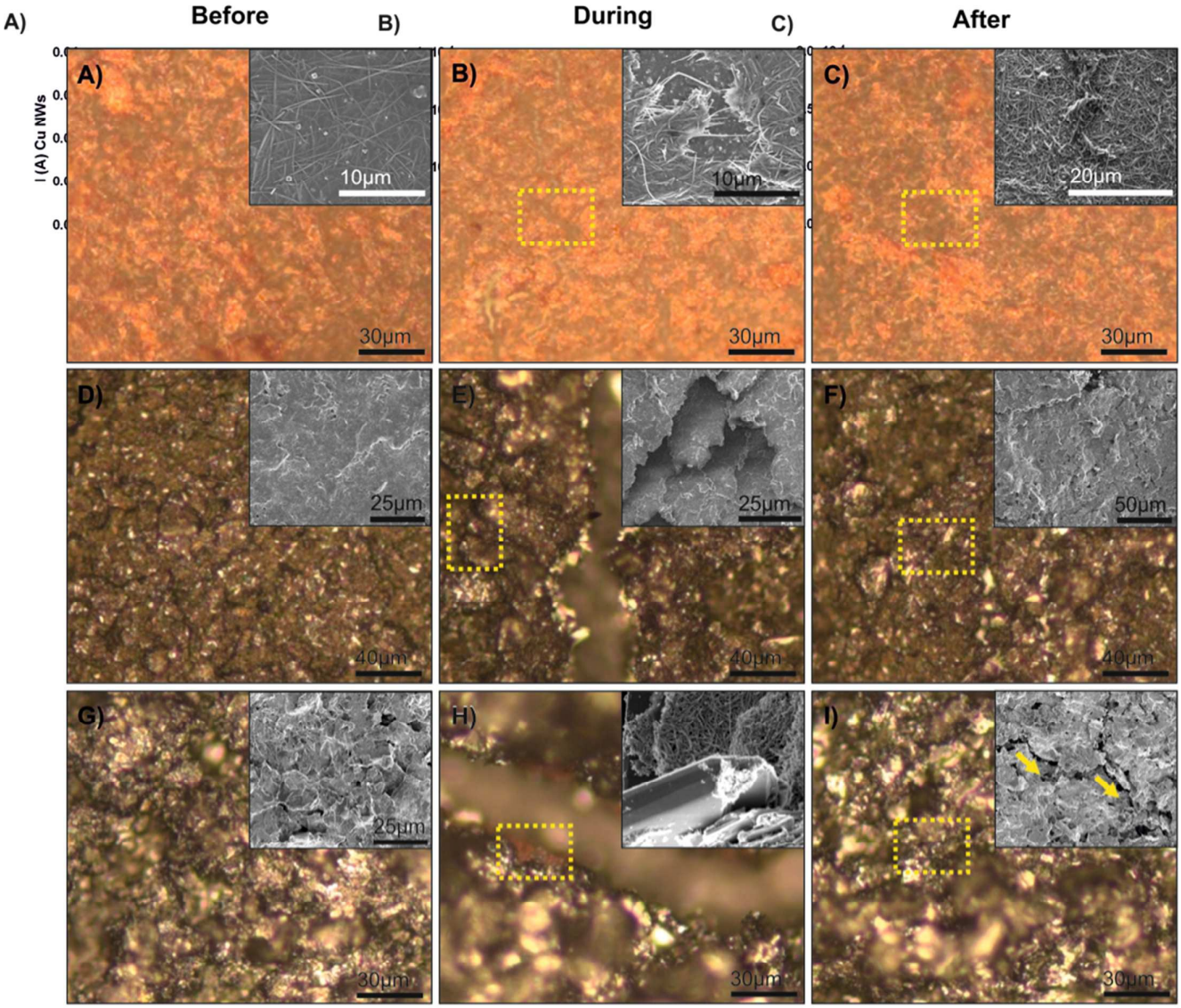

Figure 2. The 10,000 cycles test at 10% strain demonstrating the durability of the coatings, and making a comparison between coatings in terms of signal deterioration for (a) CuNWs, (b) GrMFs, (c) GrMFs/CuNWs/GrMFs.

View Article Online
DOI: 10.1039/C6NR04056J

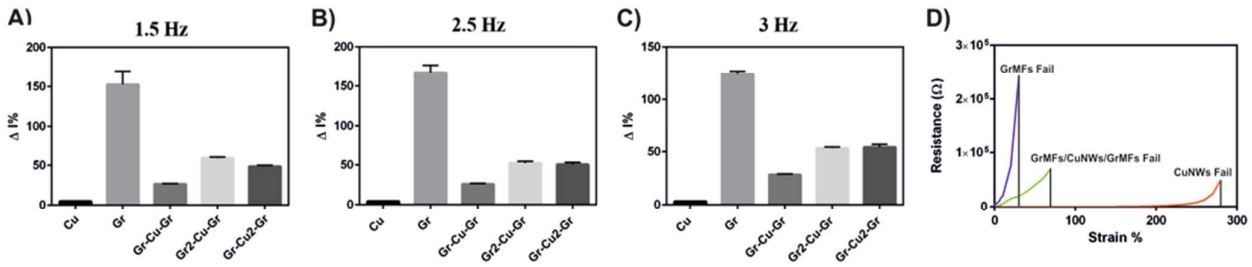

Figure 3. (a, b, c)Histograms comparing sensitivities of different coatings (for the linear shape) and showing the influence of varying frequencies. This is to determine the most sensitive coating to detect sharp and minute movements.(d) The failure strain limit of the various conducive coatings.

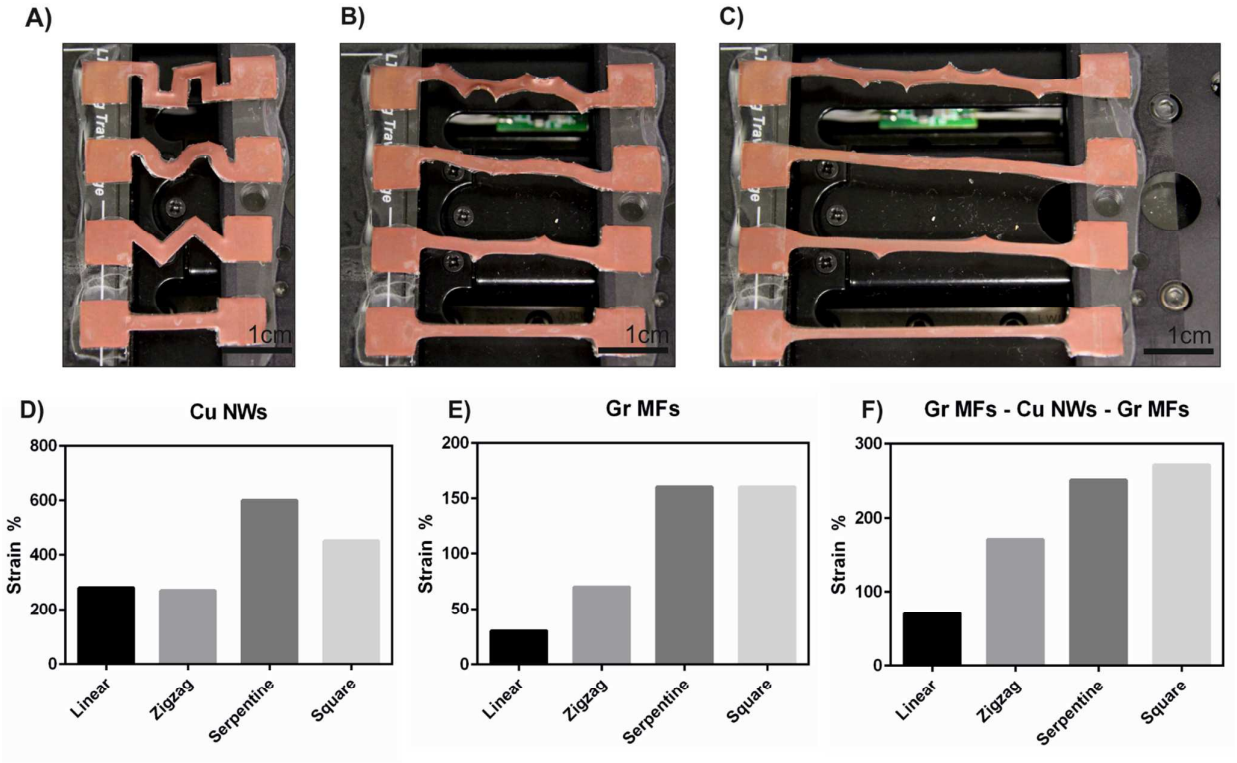

Figure 4. The fractal shapes linear, zigzag, serpentine and square being painted with CuNWs at (a) 0% strain (b) 100% strain, and (c) at 200% strain respectively. The strain range of the different shapes influenced by the different conductive paints; (d) CuNWs, (e) GrMFs, (f) GrMFs/CuNWs/GrMFs.

View Article Online
DOI: 10.1039/C6NR04056J

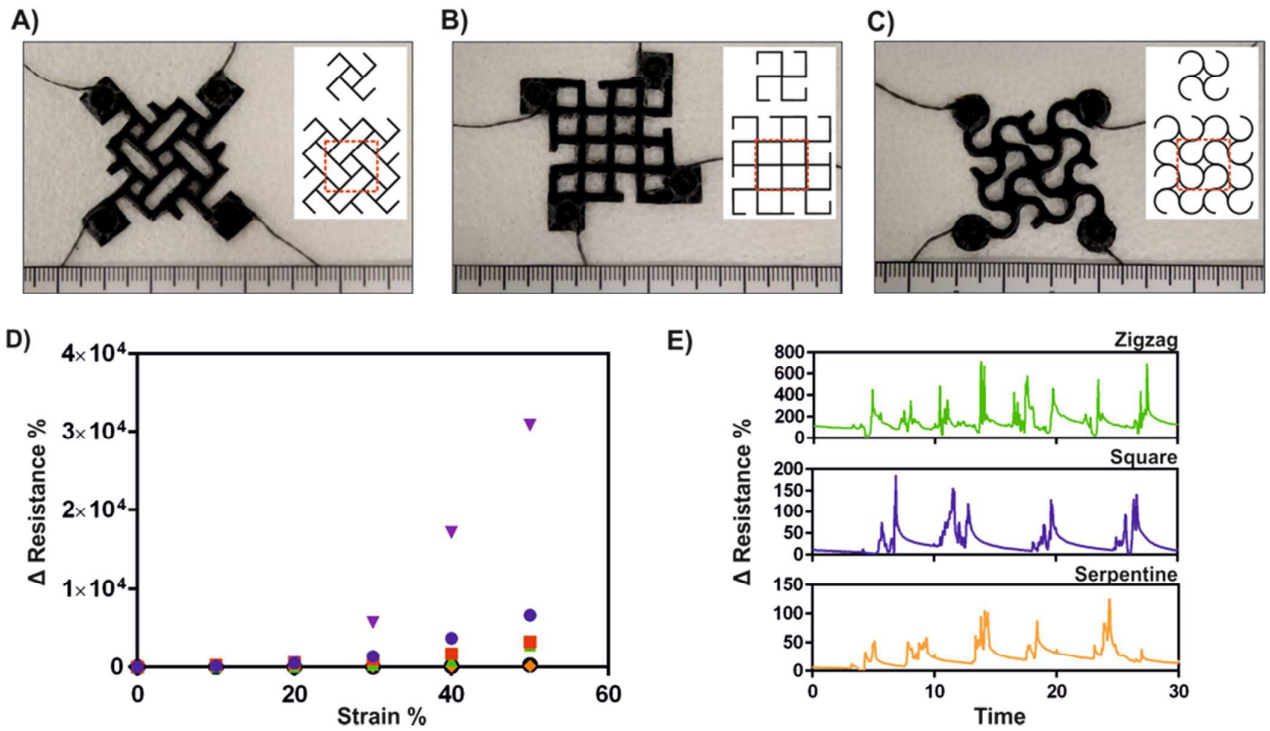

Figure 5. The second order fractal pattern biaxial and torsion GrMFs sensors with the first and second order patterns in the inset schematics. (a) zigzag, (b) square, (c) serpentine. (d) Resistance changes due to strain in the "X"-ε(11) and "Y"-ε(22) axes. The green triangles are x-zigzag, purple triangles are y-zigzag. Blue circles are x-square, red squares y-square. Orange diamonds are x-serpentine, black circles y-serpentine. (e) Shows response for random twists, ε(12) of the sensors.

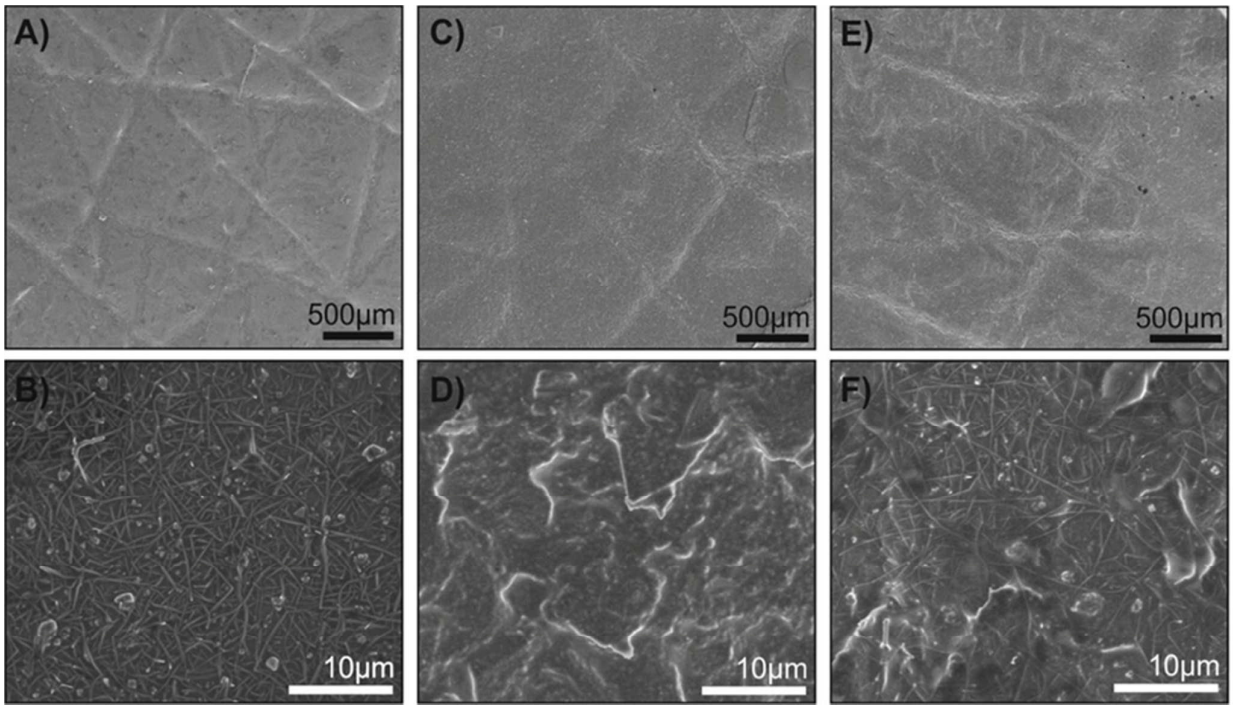

Figure 6. The conductive paints shown to be intimately contacting the many wrinkles and folds on an ecoflex replica of human skin.(a) CuNWs, (c) GrMFs, and (e) CuNWs-GrMFs and the respective magnifications in (b, d, f).

View Article Online
DOI: 10.1039/C6NR04056J

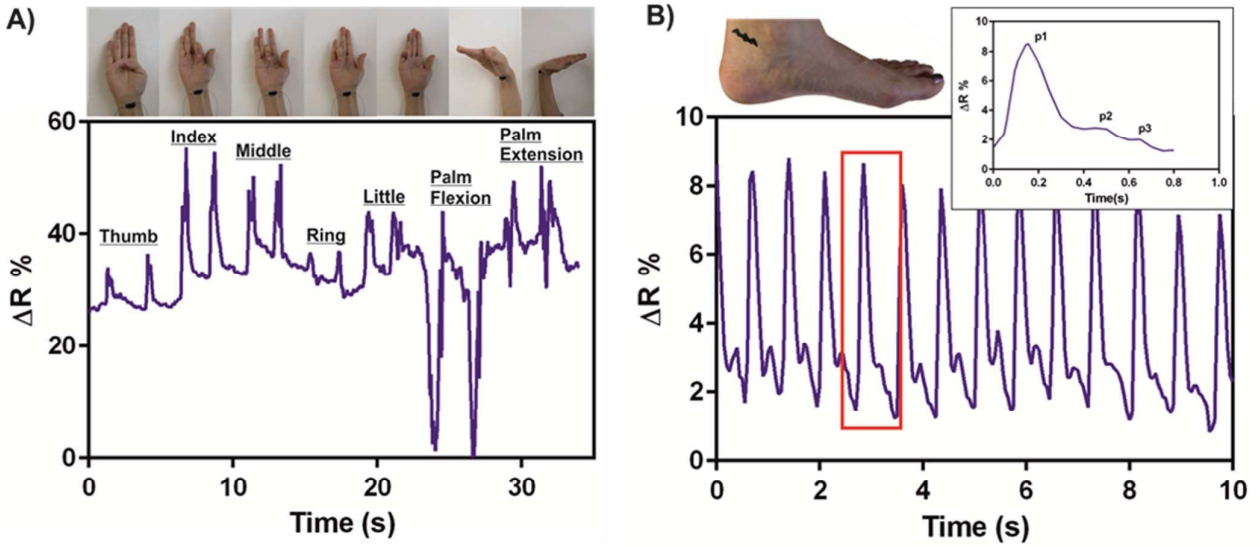

Figure 7. (a) Demonstration of single GrMFs sensor painted directly on inner wrist used to detect and differentiate between individual finger motions and hand movements. (b) GrMFs ink painted on the posterior tibial artery site in the shape of a bat shaped tattoo to detect ankle brachial artery pulse. The inset showing the pulse wave.

View Article Online
DOI: 10.1039/C6NR04056J

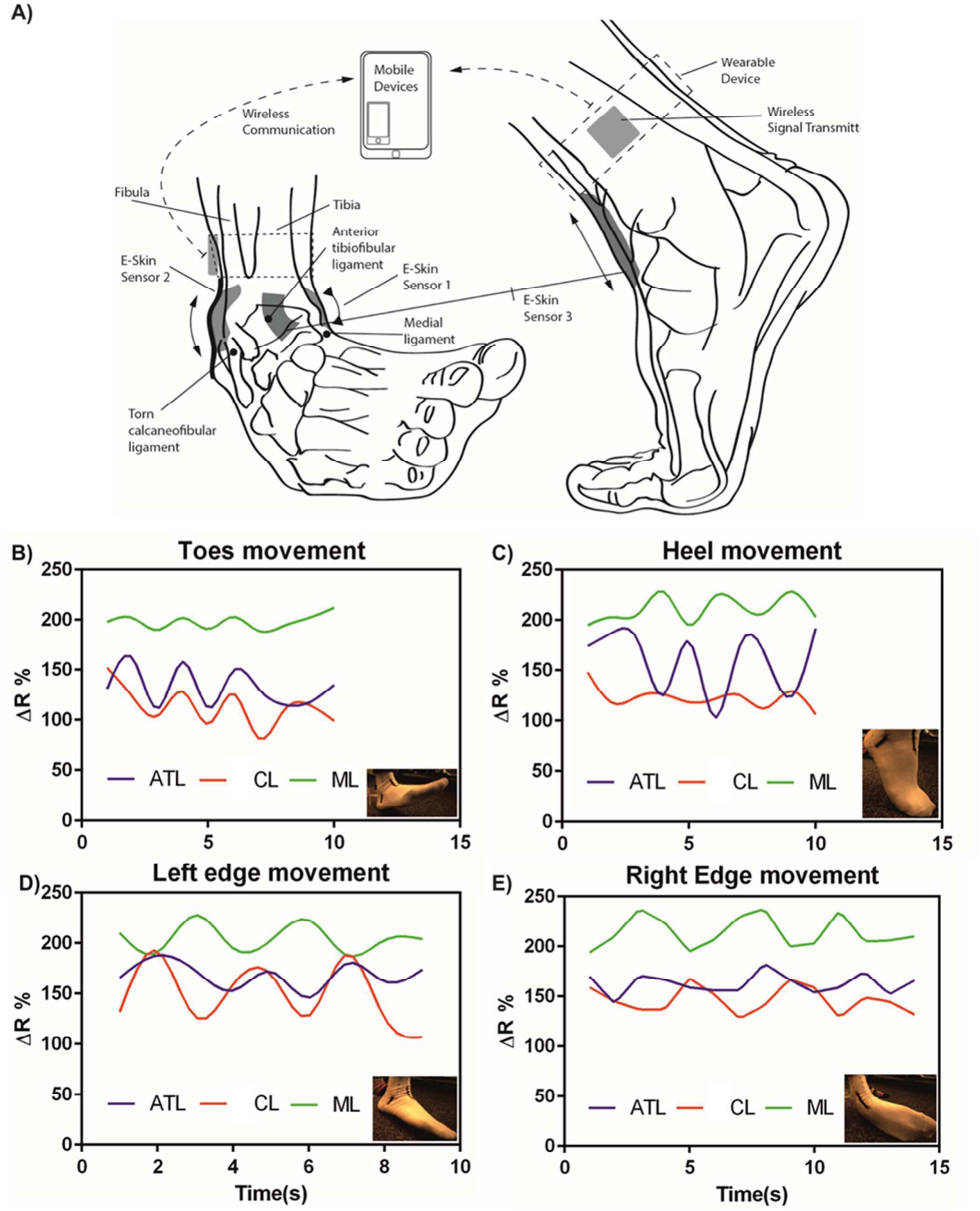

Figure 8. (a) Schematic depicting the placement of the CuNWs/GrMFs/CuNWs sensors on the ankle skin locations corresponding to the Anterior Tibiofibular Ligament (ATL), Calcaneofibular Ligament (CL), and the Medial Ligament (ML). The wireless device placed on the sensory sock can communicate to smart devices and deliver data in real time. Ankle motion sensors with the wireless platform demonstrating, (a) toes and (b) heel up-down movement, and side-to-side hinge movement on the (c) left and (d) right foot edge, and their corresponding resistance change readouts from the ankle sensor set.

View Article Online
DOI: 10.1039/C6NR04056J

Skin Inspired Fractal Strain Sensors Using a Copper Nanowires and Graphite Microflakes Hybrid Conductive Network.

Supporting Information

Naveen Noah Jason, Stephen Jia Wang, and Wenlong Cheng

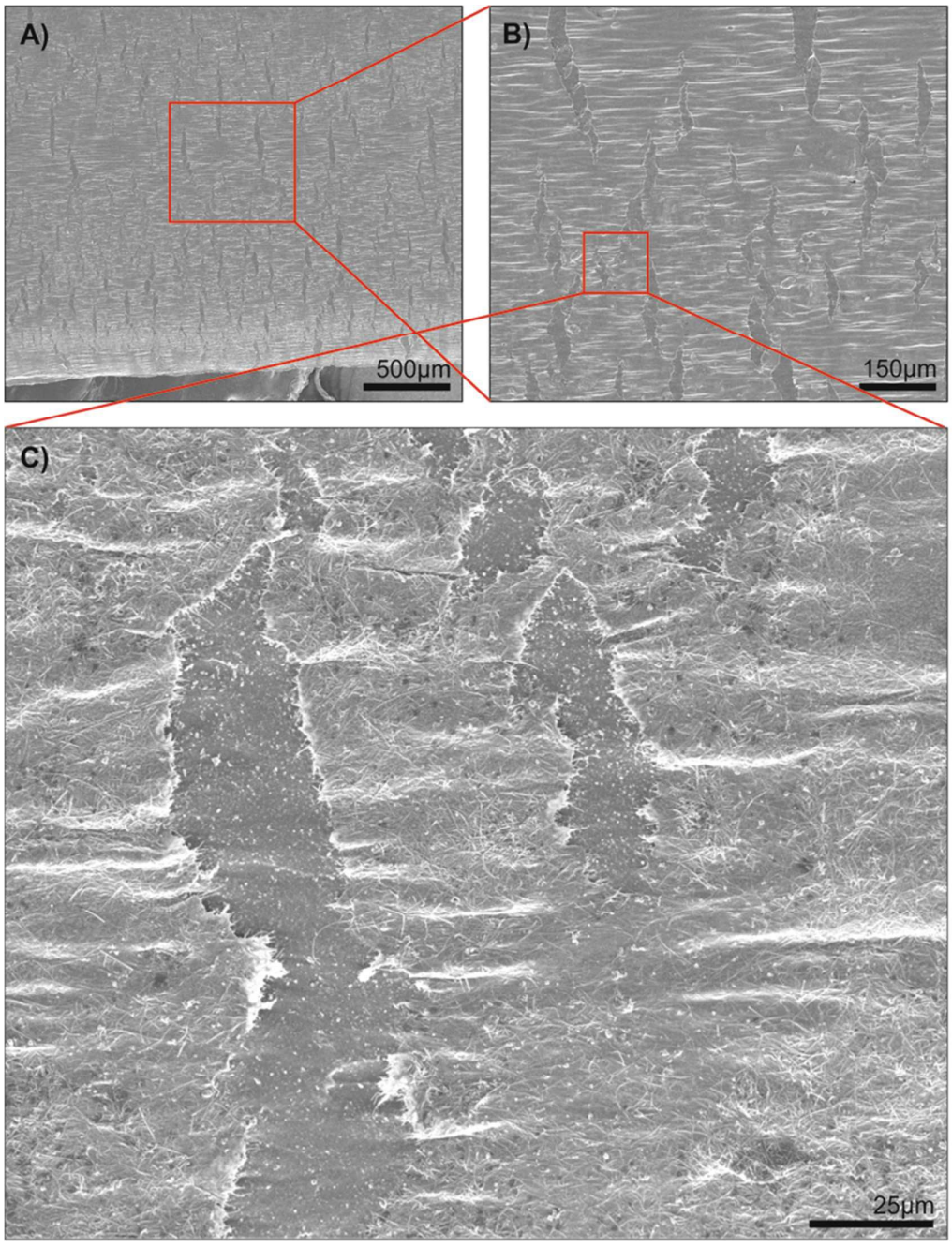

Figure S1. (a) Transversal compressional wrinkles parallel to the strain direction, and (b) longitudinal tears perpendicular to strain direction. The magnified image in (c). Perfect example of Poisson effect on unsealed nanowires film under strain.

View Article Online
DOI: 10.1039/C6NR04056J

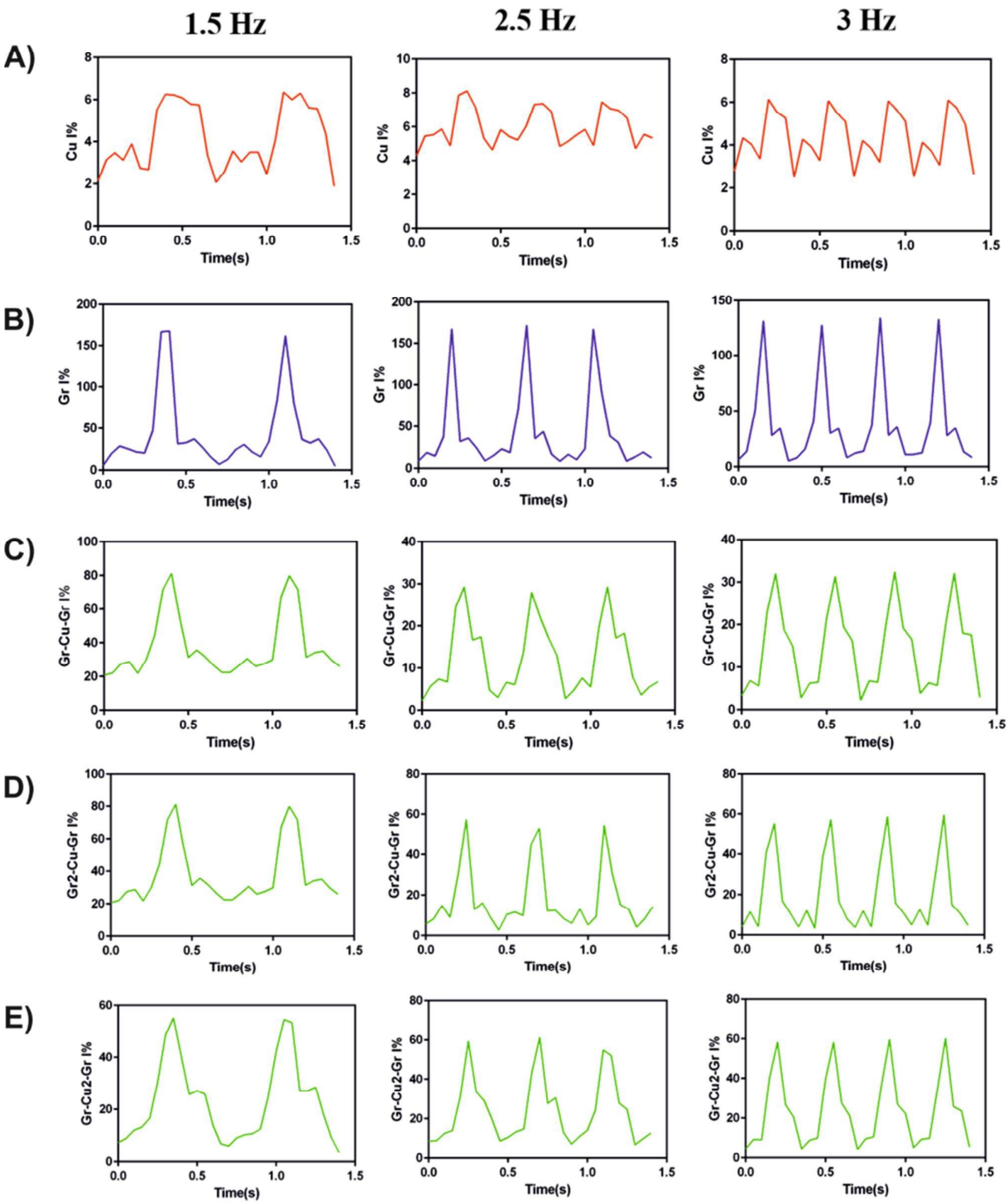

Figure S2. The distinct waveforms made by the individual coatings (on the linear shape) at different operating frequencies for (a) CuNWs, (b) GrMFs, (c) GrMFs/CuNWs/GrMFs, (d) Gr2MFs/CuNWs/GrMFs, (e) GrMFs/Cu2NWs/GrMFs.

View Article Online
DOI: 10.1039/C6NR04056J

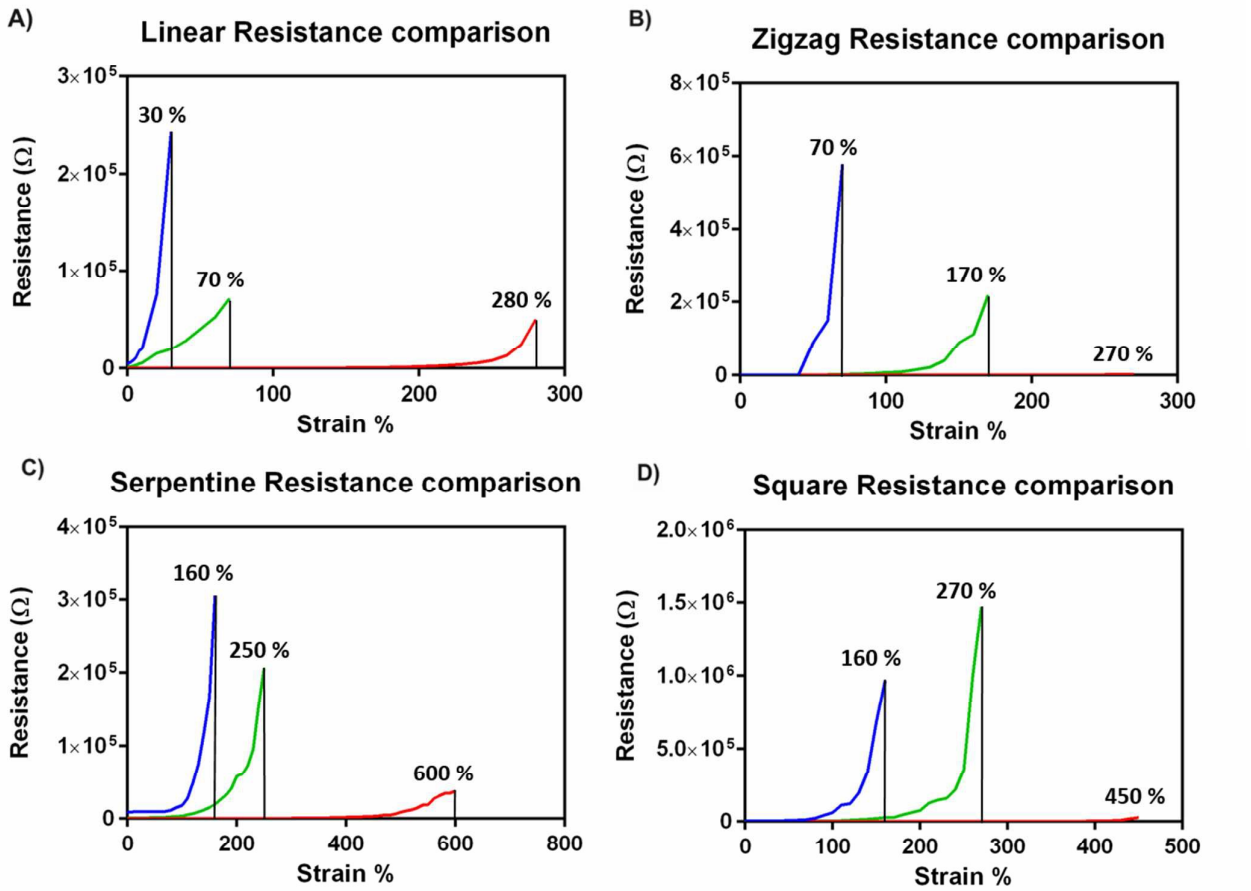

Figure S3. Comparison between the failure strains and sensitivities for different shapes with different conductive inks. This is considered as the maximum strain range for the sensors. (a) linear, (b) zigzag, (c) serpentine, (d) square. The blue plot is for GrMFs ink, red for CuNWs ink, and the green for the hybrid ink; GrMFs/CuNWs/GrMFs.

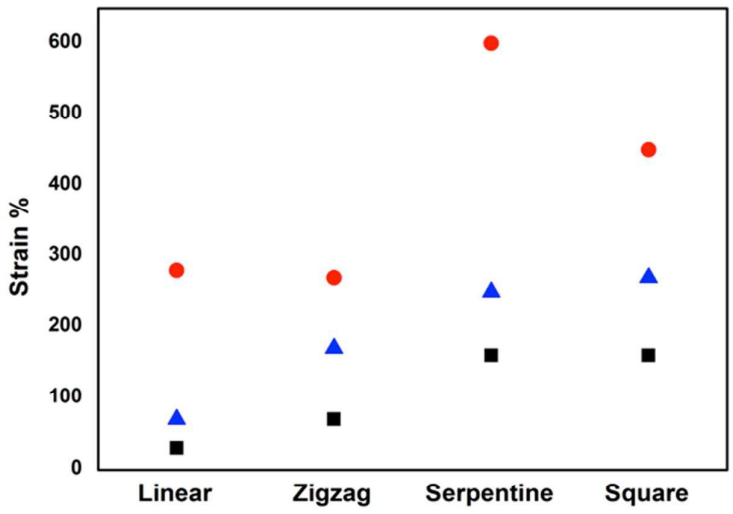

Figure S4. Curves showing the trend of shape Vs strain range, under influence of different conductive coatings. The red dots are CuNWs ink, black squares are GrMFs ink, and blue triangles are the hybrid ink; GrMFs/CuNWs/GrMFs.

View Article Online
DOI: 10.1039/C6NR04056J

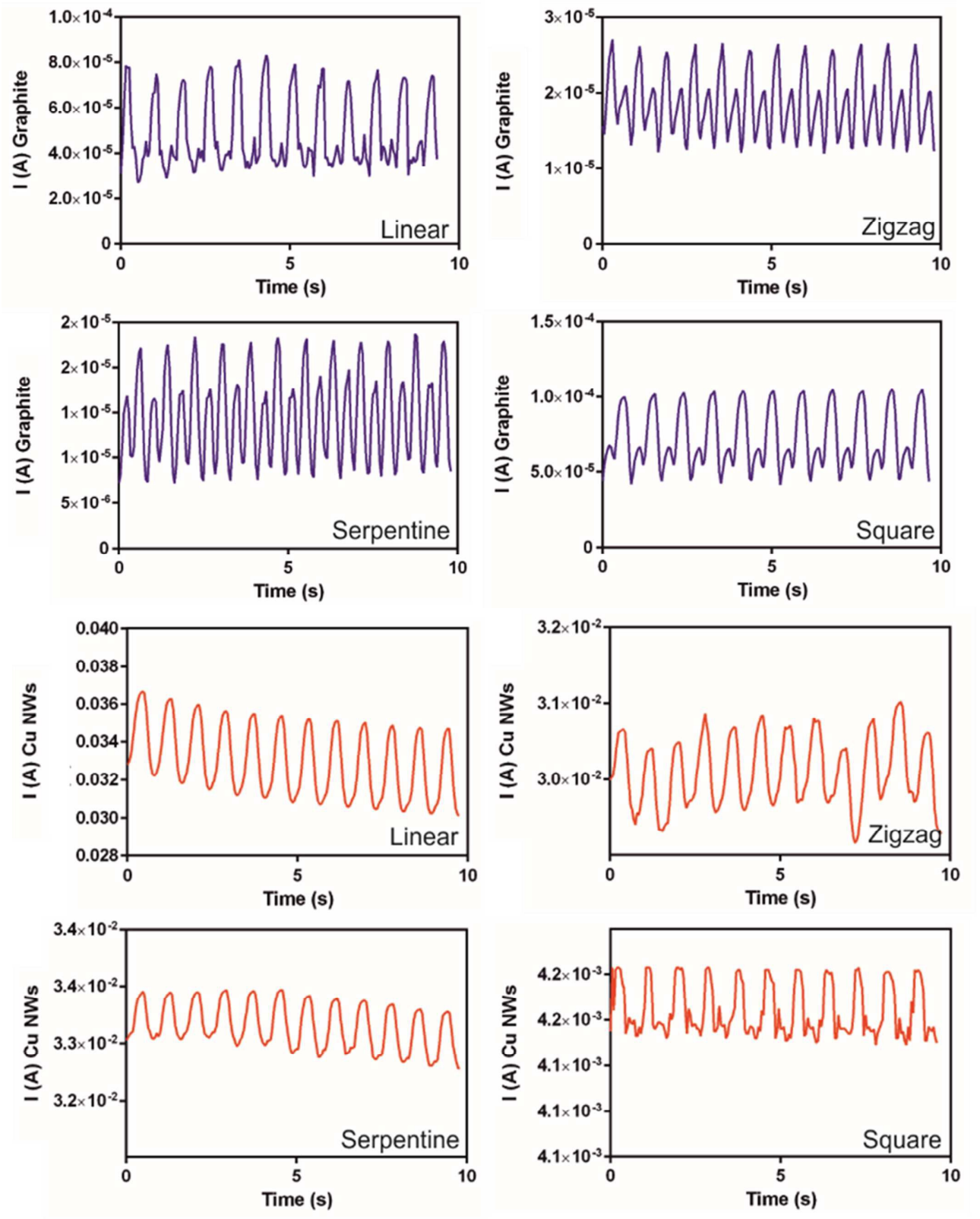

View Article Online
DOI: 10.1039/C6NR04056J

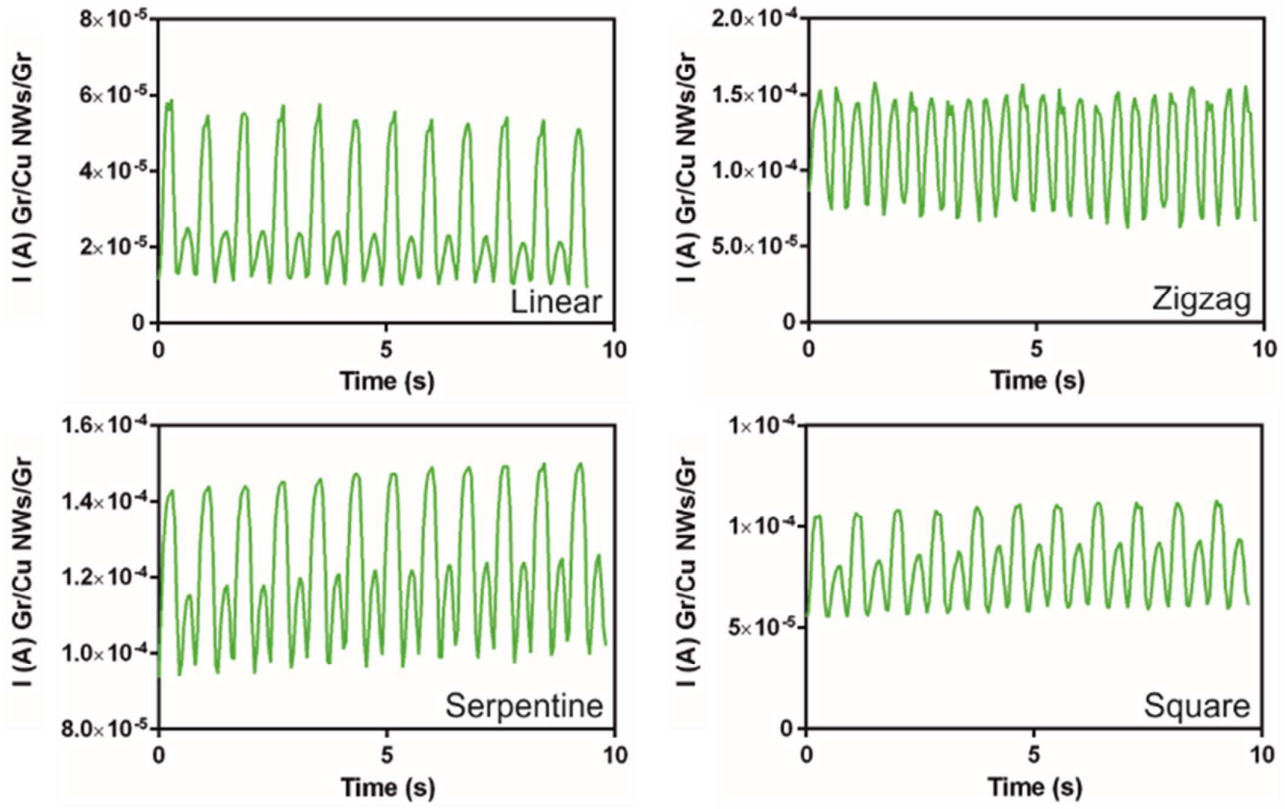

Figure S5. The influence on the distinct waveforms of the different fractal shapes on changing the conductive coatings. The blue waves are GrMFs, the red waves CuNWs, and the green waves are hybrid conductive ink; GrMFs/CuNWs/GrMFs coated.

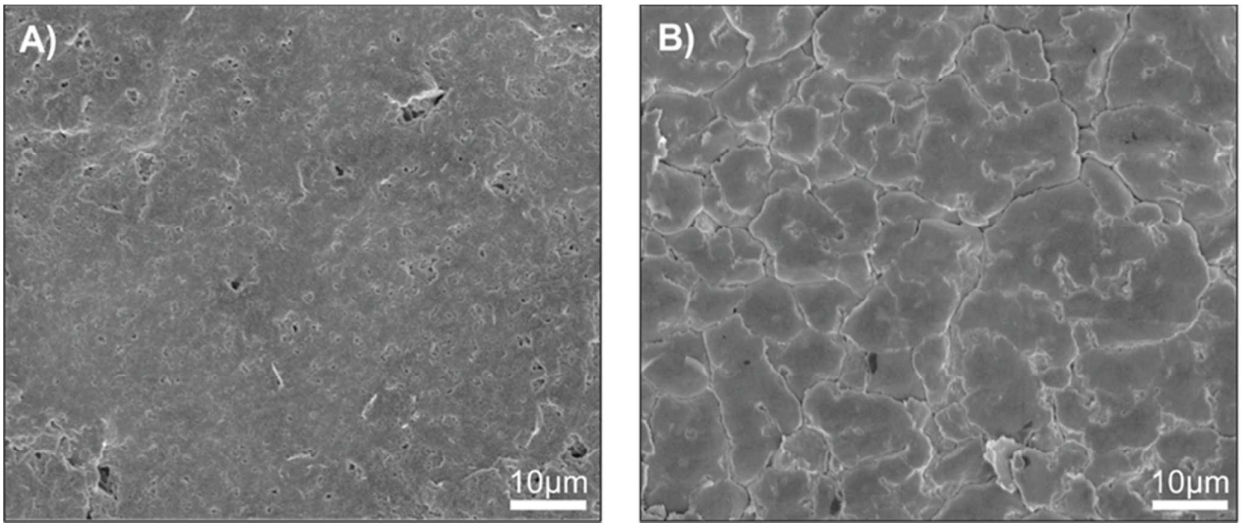

Figure S6. The smooth arrangement of graphite flakes when applied as an (a) aqueous paint compared to being rubbed on a substrate as a (b) pencil lead.

View Article Online
DOI: 10.1039/C6NR04056J

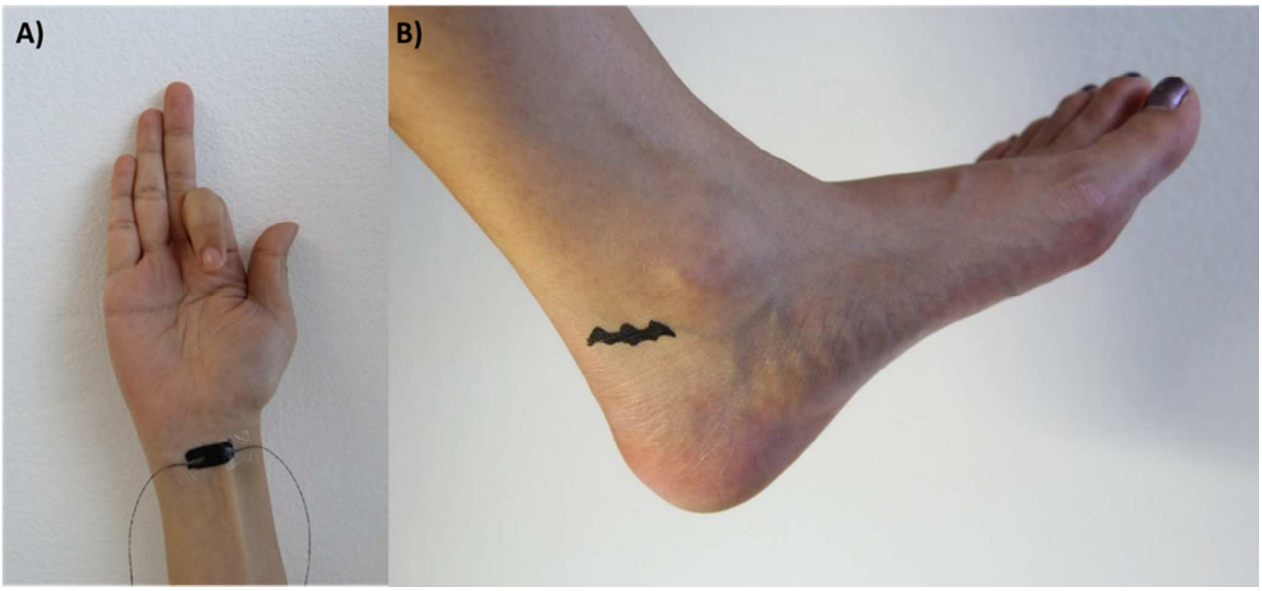

Figure S7. (a) The GrMFs ink painted onto the inner wrist to detect finger motions, and (b) painted as a bat shaped tattoo in the ankle to detect the ankle brachial pulse.

Table of Contents graphic

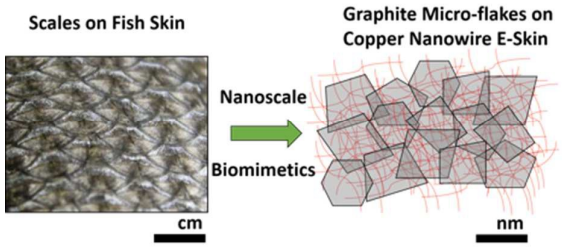

Graphite micro-flakes on copper nanowires electronic skin, emulating fish scales on biological skin.